Computational Materials Science 162 (2019) 245–254

Contents lists available at ScienceDirect

Computational Materials Science

journal homepage: www.elsevier.com/locate/commatsci

# Understanding the role of general interfaces in the overall behavior of composites and size effects

Soheil Firooz, Ali Javili*

*Department of Mechanical Engineering, Bilkent University, 06800 Ankara, Turkey*

ARTICLE INFO

*Keywords:*
General interface
Elastic interface
Cohesive interface
Size effects
Composites
Homogenization

ABSTRACT

The objective of this contribution is to investigate the role of generalized interfaces in the overall response of particulate composites and the associated size effects. Throughout this work, the effective properties of composites are obtained via three-dimensional computational simulations using the interface-enhanced finite element method for a broad range of parameters. The term interface corresponds to a zero-thickness model representing the interphase region between the constituents and accounting for the interfaces at the micro-scale introduces a physical length-scale to the effective behavior of composites, unlike the classical first-order homogenization that is missing a length-scale. The interface model here is general in the sense that both traction and displacement jumps across the interface are admissible recovering both the cohesive and elastic interface models. Via a comprehensive computational study, we identify extraordinary and uncommon characteristics of particle reinforced composites endowed with interfaces. Notably, we introduce the notion of *critical size* at which the overall behavior, somewhat surprisingly, shows no sensitivity with respect to the inclusion-to-matrix stiffness ratio. Our study, provides significant insight towards computational design of composites accounting for interfaces and in particular, nano-composites.

## 1. Introduction

In the past decades, composites have played a promising role in a broad variety of applications hence, resulting in a large body of literature on the topic. The overall behavior of composites mainly depends on their underlying micro-structure or more specifically, on distribution, volume fraction, orientation and shape of their constituents at the micro-scale. Thus, predicting the effective response of composites is a challenging task and requires sophisticated techniques such as homogenization pioneered by Hill [1] and Ogden [2]. This technique mainly relies on the two assumptions of (i) energy equivalence between the micro- and macro-scales also known as Hill–Mandel condition [3] and (ii) separation of scales. At the micro-scale, the boundary value problem often corresponds to a representative domain, referred to as the representative volume element RVE, see [4–7] for further details. Homogenization can be categorized into analytical approaches and computational methods. Analytical models have been developed in the pioneering works [8–14] and later extended in [15–20], among others. Analytical homogenization usually requires certain simplifications and, in general, cannot resolve complex microstructures leading to the need for computational methods. Computational homogenization [21–25] has been thoroughly investigated and adopted for various applications in the past decades, and reviewed in [26–29]. See Firooz et al. [30] for a detailed study on both computational and analytical homogenization as well as the influence of boundary conditions and RVE types on the overall behavior of composites. A major shortcoming of the classical computational homogenization is that it fails to account for size-dependent material behavior, often referred to as *size effects*. On the other hand, the size effects in composites are essentially attributed to surface [31] and interface effects [32,33] leading to significant properties of nano-materials due to their pronounced area-to-volume ratio, see [34–38] among others. Therefore, it is important to extend the computational homogenization method to account for the interfaces between the constituents of a micro-structure so as to capture the size effects. Homogenization and localization of nano-porous composites accounting for surface effects is reviewed in [39] illustrating size-dependent effective properties.

A trivial assumption to describe the bonding between the constituents at the micro-scale is perfect bonding. However, the assumption of perfect bonding between the constituents is usually inadequate to describe the mechanical behavior and physical nature of interfaces and therefore, imperfect interface models have been developed. The imperfect interface models can be divided into three categories of cohesive, elastic and general interfaces based on their mechanical behavior.

* Corresponding author.
*E-mail addresses:* soheil.firooz@bilkent.edu.tr (S. Firooz), ajavili@bilkent.edu.tr (A. Javili).

https://doi.org/10.1016/j.commatsci.2019.02.042
Received 28 November 2018; Received in revised form 25 February 2019; Accepted 26 February 2019
Available online 07 March 2019
0927-0256/ 

The *elastic interface model* [40–43] allows for a traction jump across the interface due to elasticity along the interface [44] but the interface remains geometrically coherent. Benveniste and Miloh [45], derived the elastic interface conditions based on a formal asymptotic expansion for the stresses and displacements of a thin interphase layer. Sharma et al. [34] used a variational formulation to derive explicit expressions for the elastic state of eigenstrained spherical inclusions embedded in a matrix with elastic interfaces. Later, Sharma and Ganti [46] proposed closed-form expressions for the modified Eshelby's tensor for cylindrical and spherical inclusions in composites with elastic interfaces, followed by Duan et al. [47]. Exploiting the composite sphere assemblage (CSA) method, the Mori–Tanaka method and the generalized self-consistent method, Duan et al. [48] established a generalized micro-mechanical framework to account for interface stress effects on the effective moduli of composites containing nano-inhomogeneities, see also [49] for nano-voids. Huang and Sun [50] obtained analytical expressions for the effective moduli of particulate composites with elastic interfaces via linearizing a finite deformation theory. Yvonnet et al. [51] established a numerical approach via combining the extended finite element method (XFEM) and the level set method to capture the elastic interface effects. The elastic interface model including three phases was addressed by Le-Quang and He [52] and closed-form first-order upper and lower bounds for the macroscopic elastic moduli were derived. Brisard et al. [53] applied a variational framework for polarization methods in nano-composites to determine a lower-bound on the shear modulus of a nano-composites with elastic interfaces. Kushch et al. [54] obtained a complete solution via vectorial spherical harmonics for the problem of multiple interacting spherical inclusions. Chatzigeorgiou et al. [55], using the theory of surface elasticity, developed a homogenization framework to account for size effects at small scales via endowing the interfaces with their own energetic structure. Dai et al. [56] used a complex variable method to obtain the effective shear modulus and the corresponding stress distribution in a composite embedding an elastic interface. Gao et al. [57] studied the effects of a curvature-dependent interfacial energy on the overall elastic properties of nano-composites. The *cohesive interface model* [58–60] allows for a displacement jump across the interface while enforcing the traction continuity [61]. Benveniste [62] extended "direct" and "energy" approaches in composite to derive the effective shear modulus of particulate composites with cohesive interfaces. Achenbach and Zhu [63] studied a composite medium with cohesive interfaces between the fibers and the matrix and obtained numerical results for the stresses in the constituents. Hashin [64,65] determined the effective elastic moduli of particulate composites with cohesive interfaces on the basis of the generalized self-consistent scheme and the composite sphere assemblage method. Lipton and Vernescu [66] introduced new variational principles and bounds for the effective elastic moduli of anisotropic two-phase composites with cohesive interfaces. Duan et al. [67] derived local and average stress concentration tensors for the inhomogeneities with cohesive and elastic interface effects based on the solutions of the elastostatic problems. Tan et al. [68] determined the effective constitutive relations of particulate composites with a piecewise linear cohesive law at the interface under hydrostatic tension. Fritzen and Leuschner [69] developed a reduced order model to predict the nonlinear response of a heterogeneous medium embedding cohesive interfaces. Both the cohesive and elastic interface models can be interpreted as two limit cases of a *general interface model* [70,71] allowing for both the displacement and traction jumps across the interface. Benveniste [72] generalized the Bövik's model [73] to an arbitrarily curved three-dimensional thin anisotropic layer between the two anisotropic constituents of a composite medium and obtained a more compact form of the interface model, see also [74,75]. Gu and He [76] derived a general interface model for coupled multifield phenomena via applying Taylor's expansion to a three-dimensional curved thin interphase. Later, Gu et al. [77] derived estimates for the size-dependent effective elastic moduli of particle-reinforced composites with general interfaces. Chatzigeorgiou et al. [78] extended the composite cylinder assemblage (CCA) approach to account for general interfaces and derived a closed-form analytical solution to compute the effective interface-enhanced material response. They also compared their solution with the computational results obtained from the finite element method and showed a remarkable agreement. Further details on thermodynamics of interfaces can be found in [79–81] among others.

Although the computational framework for interface-enhanced homogenization has been established recently, the influence of general interfaces on the overall behavior of composites remains elusive and poorly understood to date, mainly due to the lack of a thorough numerical investigation on the subject. In this manuscript we present a comprehensive computational study and identify extraordinary and uncommon characteristics of particle reinforced composites due to the general interfaces at the micro-scale. The insights provided in this work are particularly important from a computational material design perspective.

## 2. Micro-to-macro transition

In this section, we briefly elaborate on the governing equations of continua embedding general interface at the micro-scale and the associated micro-to-macro transition, see [78,82] for detailed analysis. Similar to the classical first-order homogenization, it is assumed that the constitutive material behavior at the micro-scale is known and the overall response at the macro-scale is obtained via proper volume averaging at the micro-scale. But unlike the classical first-order micro-to-macro transition, the current framework possesses a physical length-scale and can account for size effects, see Fig. 1.

Consider a continuum body at the macro-scale taking the configuration ${}^{\mathrm{M}}\mathscr{B}$ corresponding to a heterogeneous medium, as shown in Fig. 1 with its underlying RVE at the micro-scale denoted $\mathscr{B}$. The microstructure is separated by the interface $\mathscr{I}$ into two disjoint subdomains $\mathscr{B}^{+}$ and $\mathscr{B}^{-}$. The outward unit normal to the boundary $\mathscr{S}$ is denoted $\boldsymbol{n}$ whereas $\overline{\boldsymbol{n}}$ defines the interface unit normal pointing from the minus to the plus side of the interface. The interface displacement $\overline{\boldsymbol{u}}$ is defined as the average displacement across the interface as $\overline{\boldsymbol{u}} := \{\{\boldsymbol{u}\}\} = \frac{1}{2}[\boldsymbol{u}^{+} + \boldsymbol{u}^{-}]$ with $\boldsymbol{u}$ being the displacement field in the bulk. Accordingly, the strain fields in the bulk and on the interface read

$$\begin{aligned}\boldsymbol{\varepsilon} &= \frac{1}{2}[\boldsymbol{i}\cdot\mathrm{grad}\boldsymbol{u} + [\mathrm{grad}\boldsymbol{u}]^{\mathrm{t}}\cdot\boldsymbol{i}] \text{ in } \mathscr{B} \quad \text{and} \quad \overline{\boldsymbol{\varepsilon}} \\ &= \frac{1}{2}[\overline{\boldsymbol{i}}\cdot\overline{\mathrm{grad}}\,\overline{\boldsymbol{u}} + [\overline{\mathrm{grad}}\,\overline{\boldsymbol{u}}]^{\mathrm{t}}\cdot\overline{\boldsymbol{i}}] \text{ on } \mathscr{I},\end{aligned} \tag{1}$$

with $\boldsymbol{i}$ being the identity tensor and $\overline{\boldsymbol{i}} = \boldsymbol{i} - \overline{\boldsymbol{n}} \otimes \overline{\boldsymbol{n}}$ the interface projection tensor. In the absence of external forces, the balance equations for the micro-scale problem in the bulk and on the interface read

$$\begin{aligned}&\mathrm{div}\boldsymbol{\sigma} = 0 \quad \text{in } \mathscr{B}, && \boldsymbol{\sigma}\cdot\boldsymbol{n} = \boldsymbol{t} \quad \text{on } \mathscr{S}, \\ &\overline{\mathrm{div}}\,\overline{\boldsymbol{\sigma}} + [[\boldsymbol{\sigma}]]\cdot\overline{\boldsymbol{n}} && \{\{\boldsymbol{\sigma}\}\}\cdot\overline{\boldsymbol{n}} \\ &\quad = 0 \quad \text{on } \mathscr{I} \text{ (along the interface)}, && \quad = \overline{\boldsymbol{t}} \quad \text{on } \mathscr{I} \text{ (acrosstheinterface)},\end{aligned} \tag{2}$$

where $\boldsymbol{t}$ and $\overline{\boldsymbol{t}}$ are the surface and interface traction vectors. The constitutive material behavior in the bulk takes the standard form $\boldsymbol{\sigma} = 2\,\mu\,\boldsymbol{\varepsilon} + \lambda\,[\boldsymbol{\varepsilon}\colon\boldsymbol{i}]\boldsymbol{i}$ where $\lambda$ and $\mu$ are the bulk Lamé parameters. On the other hand, the interface material behavior is decomposed into tangential and orthogonal parts. The *tangential* response of the general interface model is reminiscent of the *elastic* resistance in the surface elasticity theory of Gurtin and Murdoch [40] but the *orthogonal* part of the general interface behavior is similar to the *cohesive* resistance [60]. Therefore, the general interface model can be interpreted as a combination of both the elastic and cohesive interface models, see Fig. 2. The tangential constitutive law along the interface reads $\overline{\boldsymbol{\sigma}} = 2\overline{\mu}\,\overline{\boldsymbol{\varepsilon}} + \overline{\lambda}\,[\overline{\boldsymbol{\varepsilon}}\colon\overline{\boldsymbol{i}}]\overline{\boldsymbol{i}}$ with $\overline{\lambda}$ and $\overline{\mu}$ being the interface Lamé parameters similar in nature to the bulk parameters $\lambda$ and $\mu$, respectively. The

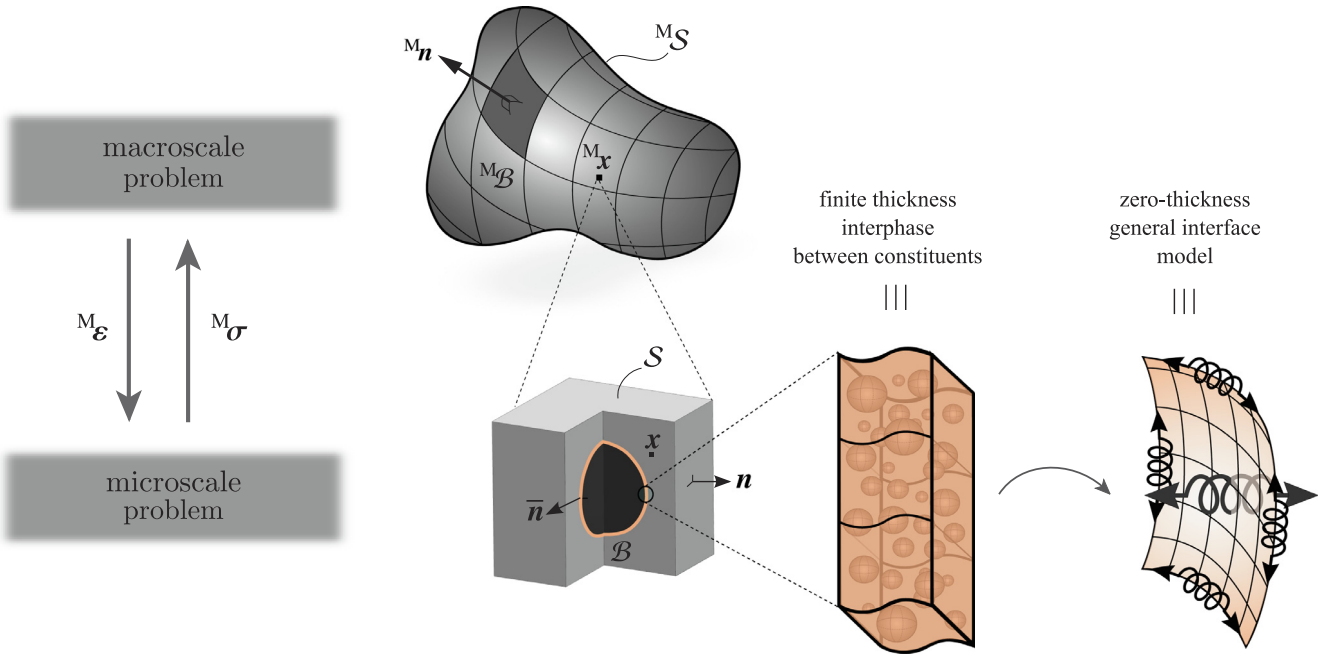


**Fig. 1.** Problem definition for homogenization accounting for the general interface model. We assume that a zero-thickness interface model can sufficiently replace a finite-thickness interphase region between the constituents.

orthogonal constitutive law across the interface reads $\bar{\boldsymbol{t}} = \bar{k}\,[[\boldsymbol{u}]]$ where $\bar{k}$ is the interface cohesive resistance against opening.

Equipped with the kinematic description, governing equations and constitutive laws, we link the behavior at the micro-scale to its macro-scale counterpart via proper volume averaging at the micro-scale. The boundary conditions at the micro-scale are chosen such that the energy equivalence between the scales is a priori fulfilled. Among various boundary conditions that sufficiently satisfy the Hill–Mandel condition, we choose the periodic boundary condition. Using the divergence theorem, macroscopic stress and strain can be expressed in terms of integrals at the micro-scale

$$\begin{aligned} {}^{\mathrm{M}}\boldsymbol{\varepsilon} &= \frac{1}{\mathcal{V}}\int_{\mathscr{B}} \boldsymbol{\varepsilon}\,\mathrm{d}V + \frac{1}{\mathcal{V}}\int_{\mathscr{S}} \frac{1}{2}[[[\boldsymbol{u}]]\otimes\ \bar{\boldsymbol{n}} + \bar{\boldsymbol{n}}\otimes\ [[\boldsymbol{u}]]]\,\mathrm{d}A, \quad {}^{\mathrm{M}}\boldsymbol{\sigma} \\ &= \frac{1}{\mathcal{V}}\int_{\mathscr{B}} \boldsymbol{\sigma}\,\mathrm{d}V + \frac{1}{\mathcal{V}}\int_{\mathscr{S}} \bar{\boldsymbol{\sigma}}\,\mathrm{d}A. \end{aligned} \tag{3}$$

## 3. Uncommon characteristics of composites due to interfaces

In this section, we elaborate on the uncommon behavior of composites due to accounting for interfaces at the micro-scale. More precisely, we investigate the effective response of particulate composites embedding general interfaces for a broad range of parameters and consequently, identify a number of extraordinary and distinctive characteristics that are present because of the interfaces, otherwise missing in the classical computational homogenization. In doing so, using our in-house finite element code, we carry out numerical simulations to study the effects of various parameters such as volume fraction, stiffness ratio, interface parameters and size on the overall material response. The inclusion-to-matrix volume fraction of the RVE is denoted $f$ and the stiffness ratio incl./matr. represents the ratio of the inclusion Lamé parameters to the matrix Lamé parameters. The two

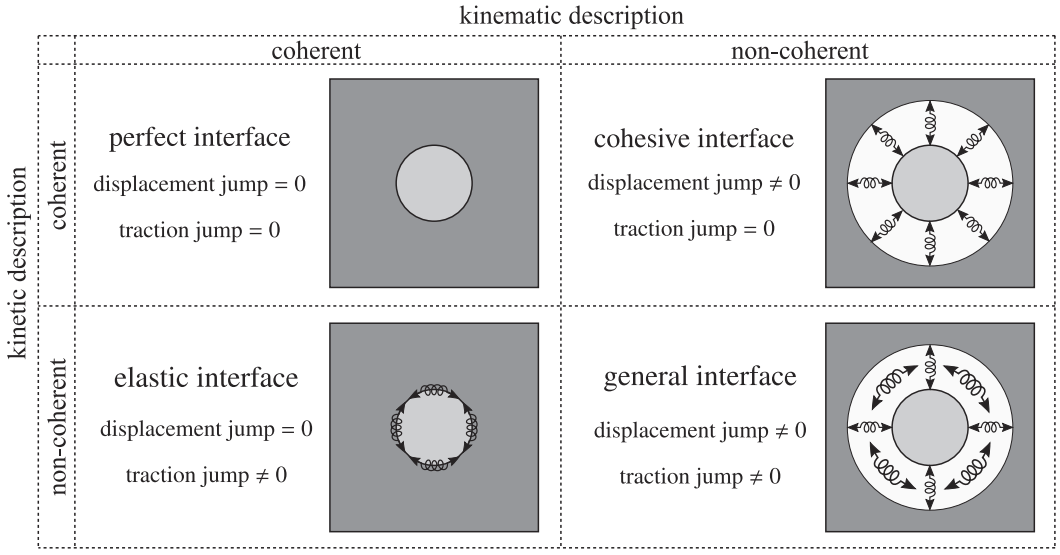


**Fig. 2.** Categorization of the interface models based on their kinematic or kinetic behavior.

limits of the stiffness ratio are incl. /matr. =0 and incl. /matr. $\to\infty$ corresponding to voids and rigid inclusions, respectively. Throughout the examples, the matrix Lamé parameters are set to $\lambda_1 = \mu_1 = 1$ and the inclusion Lamé parameters are calculated according to the prescribed stiffness ratio. The interface Lamé parameters $\overline{\lambda}$ and $\overline{\mu}$ determine the interface in-plane resistance or *interface resistance against stretch*, similar to the elastic interface model. On the other hand, the interface cohesive resistance $\overline{k}$ is associated with the interface orthogonal resistance or *interface resistance against opening*, similar to the cohesive interface model. The term *size* here corresponds to the size of the RVE or the length of each side of the RVE. Note, the numerical examples are purposefully devised so as to highlight the distinctive features of the proposed framework and therefore, the results are merely parametric studies and not tailored to any specific application or material. Therefore, the units of the parameters do not play a crucial role here as long as they are consistent keeping in mind that for instance $\overline{\mu}/\mu$ has the length dimension but $\overline{k}/\mu$ has the inverse length dimension. Finally, when providing the stress distributions within the micro-structure, different sizes are scaled for the sake of graphical presentation.

***Accounting for interfaces results in size-dependent effective material response.*** The first and most important outcome of accounting for interfaces at the micro-scale is to introduce a length-scale into computational homogenization, and hence size effects in the overall behavior of composites. The first set of examples illustrated in Fig. 3 is devised to highlight the influence of size on the overall material response in the presence of interfaces. Fig. 3 provides the effective bulk modulus versus size for two volume fractions of $f = 15\%$ and $f = 30\%$. Furthermore, it is clearly shown how in the absence of the interfaces the overall material response becomes insensitive with respect to the size of the micro-structure. Note, the area-to-volume ratio tends to zero for very large sizes, and hence identical effective properties with or without interfaces. On the other hand, the area-to-volume ratio is more significant for very small sizes leading to pronounced interface influence on the overall material behavior. However, the interface effects are not necessarily predictable. For instance, for the specific set of parameters in this example, at very small sizes the interface does not play a crucial role on the effective bulk modulus. As we will see shortly, this is not always the case and the cohesive-to-elastic interface parameters ratio as well as the incl./matr. are the decisive factors, discussed in Figs. 8–10. Finally, note that different sizes with different stress distributions at the micro-scale may result in the same effective property at the macro-scale due to interface effects, compare points 3 and 7 in Fig. 3, for instance.

***Identical material response can be obtained at two different volume fractions.*** Another surprising outcome of accounting for general interfaces at the micro-scale is to obtain identical effective properties for different volume fractions, for a fixed set of parameters. Note, the effective response is directly related to the volume fraction in the absence of interfaces. More precisely, for a fixed set of material parameters, changing the volume fraction inevitably results in different effective properties according to the classical computational homogenization. However, that is not the case here due to the presence of the interfaces at the micro-scale. Fig. 4 depicts the effective bulk modulus with respect to size for two different volume fractions $f = 15\%$ and $f = 30\%$. The distribution of the $xx$-component of the stress in the micro-structure due to volumetric expansion is depicted for the sizes where their effective bulk moduli coincide. This observation is particularly important since it allows us to reduce the volume fraction with no compromise on the effective behavior.

***Identical overall response at different volume fractions is only attainable if interface parameters are significant.*** As pointed out previously, in the presence of general interfaces at the micro-scale it is possible to obtain identical effective properties at different volume fractions, for a fixed set of parameters. However, this extraordinary behavior can only be observed if the interface parameters are large enough. Fig. 5 examines the influence of various interface parameters on the overall material behavior for two different volume fractions $f = 15\%$ and $f = 30\%$. If the interface does not contribute sufficiently to the overall response, the effective properties corresponding to $f = 15\%$ always overestimate those associated with $f = 30\%$. But, if the interface influence is significant enough, the effective bulk modulus associated with $f = 30\%$ overestimates that of $f = 15\%$ for a certain range of sizes resulting in the two lines intersecting each other at two sizes depending on the material parameters.

***Cohesive and elastic interface models recovered as limits of the***

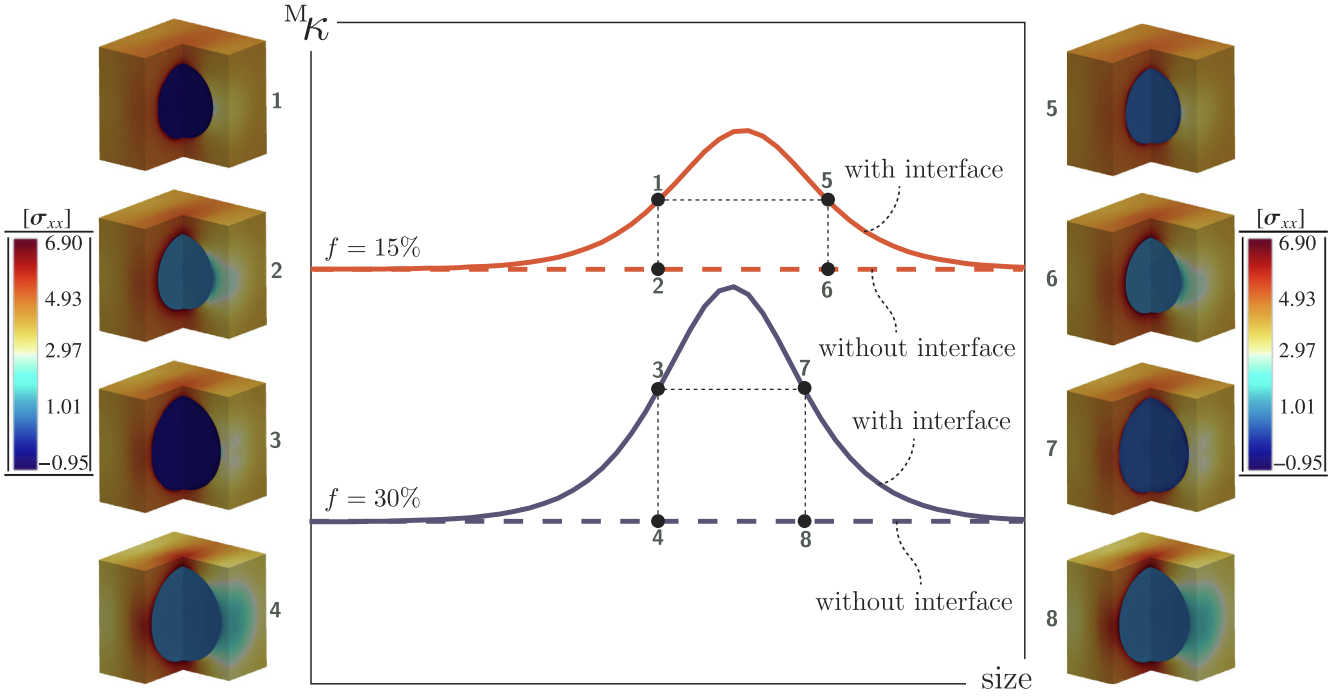


**Fig. 3.** Size-dependent material response due to the presence of general interfaces at the micro-scale for two different volume fractions. The general interface parameters are $\overline{\lambda} = \overline{\mu} = 1$ and $\overline{k} = 1$ and the stiffness ratio is 0.1.

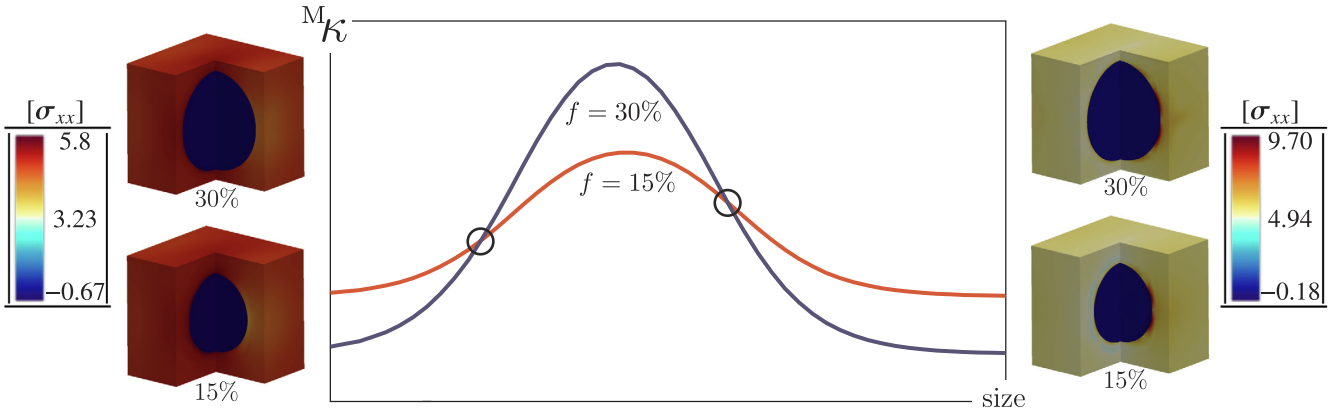


**Fig. 4.** Effective bulk modulus versus size for different interface parameters. The stiffness ratio is 0.1 and the general interface parameters are $\overline{\lambda} = \overline{\mu} = 1$ and $\overline{k} = 100$. The distribution of the *xx*-component of the stress throughout the RVE is depicted for the points that the results coincide.

***general interface model.*** As pointed out previously, the general interface model allows for both the displacement and traction jumps across the interface and thus, shall be understood as the combination of the elastic and cohesive interface models. Consequently, one expects to recover both the elastic and cohesive interface model as limits of the general interface model. Fig. 6 illustrates the overall bulk modulus and shear modulus $^{M}\kappa$ and $^{M}\mu$, respectively, for a broad range of interface material parameters. The interface parameters $\overline{\lambda}$ and $\overline{\mu}$ correspond to the resistance along the interface against stretch but $\overline{k}$ correspond to the resistance across the interface against opening. Obviously, when $\overline{\lambda} = \overline{\mu} = 0$, the interface in-plane resistance vanishes and $\overline{k}$ would be the only remaining interface parameter and thus, the general interface model coincides with the cohesive interface model. On the other hand, when $\overline{k} \to \infty$ or $1/\overline{k} \to 0$, the displacement jump across the interface vanishes resulting in a coherent interface with resistance along the interface reminiscent of the elastic interface model. The intersection of both the cohesive and elastic interface models is a point representing the perfect interface model for which both the displacement and traction jumps across the interface vanish.

***The larger the interface parameters, the stiffer the effective response.*** We study the influence of the general interface parameters on the overall material response next. Fig. 7 illustrates the significance of the general interface parameters on the overall properties of composites and the stress distribution in the micro-structure. In particular, this figure shows that the interface parameters are essentially stiffness-like parameters in the sense that larger values of the interface parameters result in stiffer macroscopic behavior. More precisely, larger $\overline{k}$ results in larger effective parameters $^{M}\kappa$ and $^{M}\mu$ for any set of $\overline{\lambda}$ and $\overline{\mu}$. Similarly, larger $\overline{\lambda}$ and $\overline{\mu}$ result in larger effective parameters $^{M}\kappa$ and $^{M}\mu$ for any $\overline{k}$. That is, the most compliant overall behavior can be obtained if all the interface parameters vanish altogether or oppositely, the larger the interface parameters, the stiffer the effective response.

***General interface model results in a critical size where the overall response is independent of the stiffness ratio.*** When accounting for the general interface model at the micro-scale, for any fixed set of interface parameters, there exists a *critical size* $\ell_c$ at which the effective response of the composite is independent of the stiffness ratio as illustrated in Figs. 8–10 for three different sets of interface parameters. Figs. 8–10

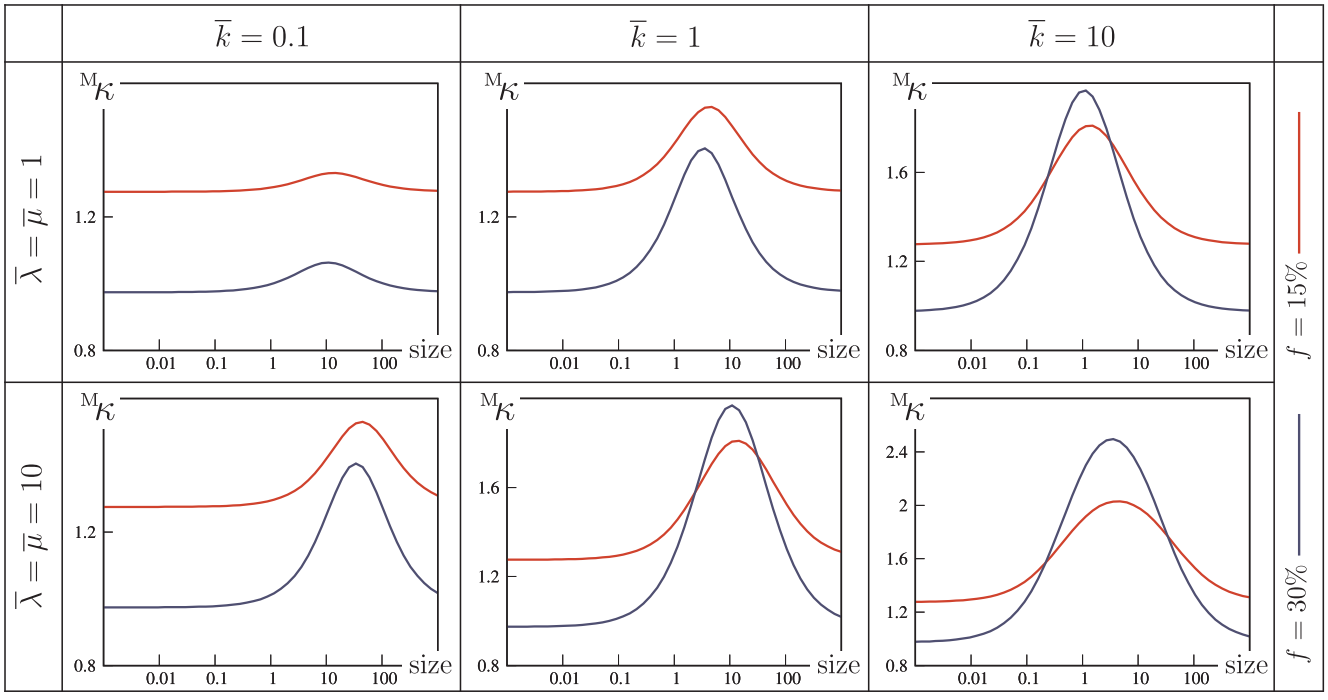


**Fig. 5.** Effects of interface parameters on the overall material behavior.

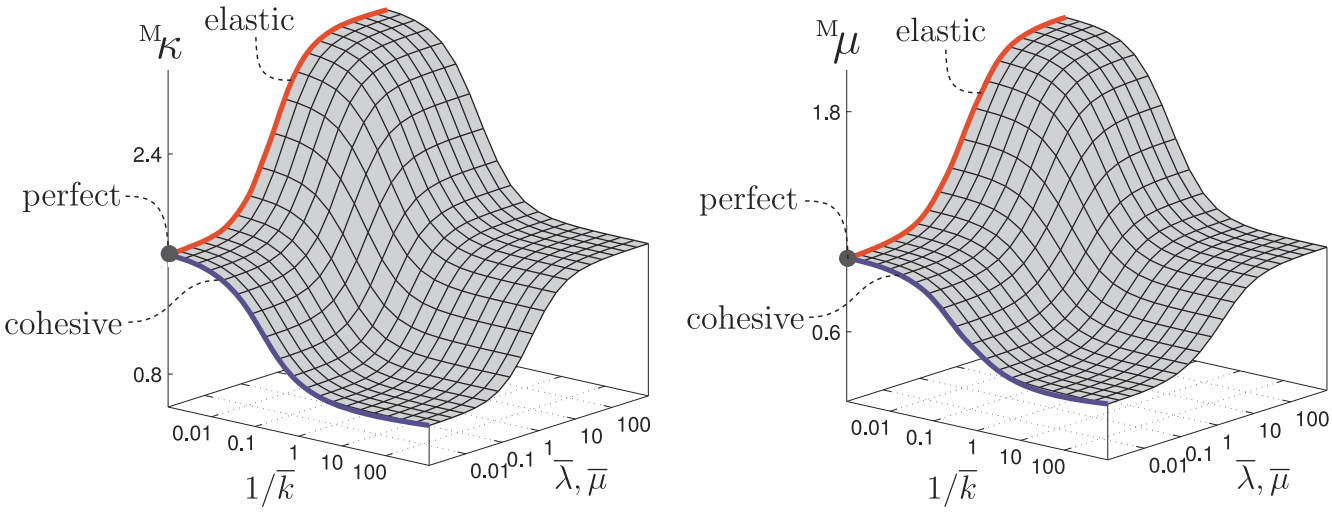


**Fig. 6.** Cohesive and elastic interface models are recovered as the limits of the general interface model. The stiffness ratio is 1 and the volume fraction is $f = 30\%$.

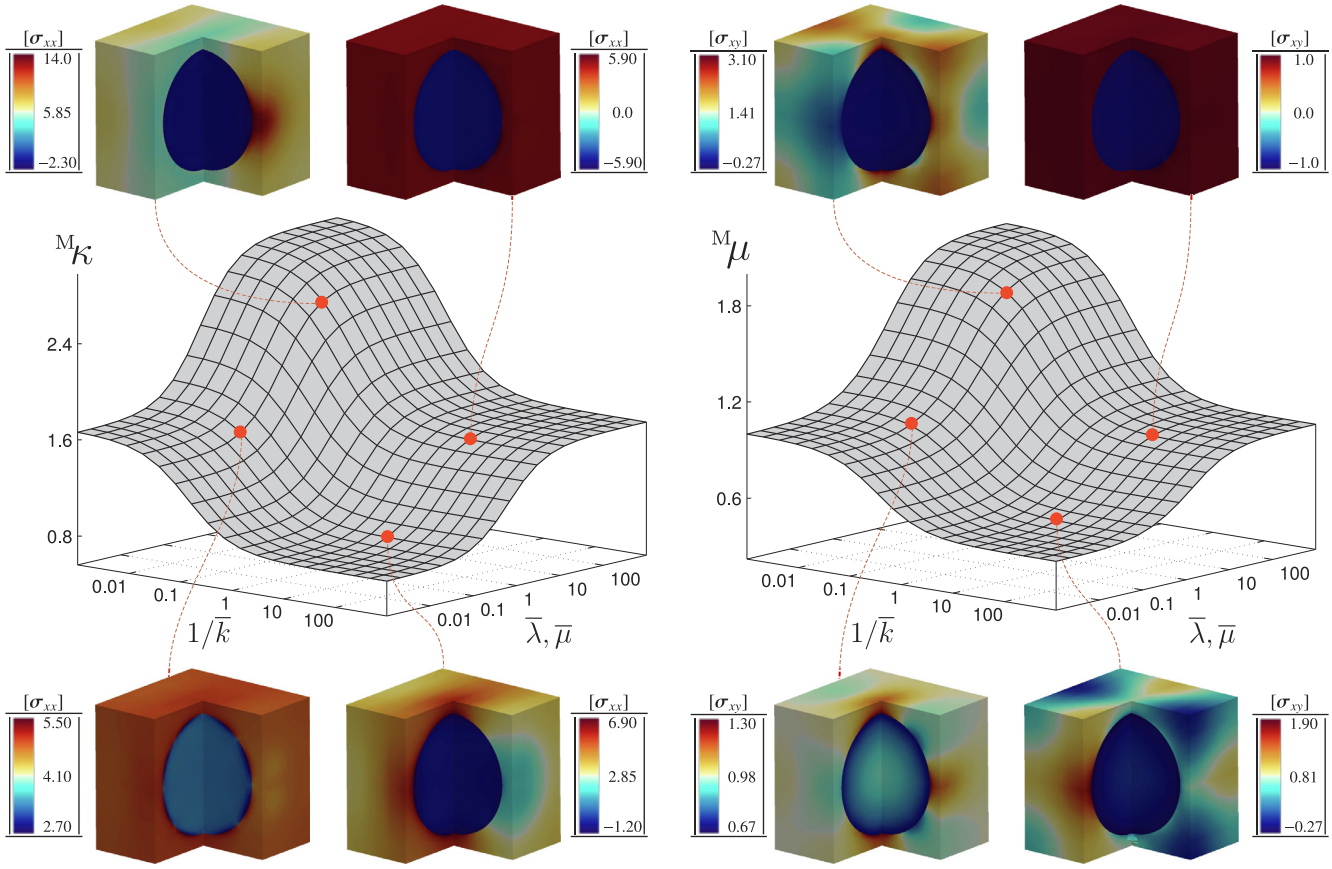


**Fig. 7.** Contribution of the general interface parameters in the overall effective properties. On the left, the distribution of the *xx*-component of the stress throughout the RVE due to volumetric expansion is shown for the general interface at size = 1. On the right, the distribution of the *xy*-component of the stress throughout the RVE due to simple shear is shown for the general interface at size = 1. The stiffness ratio is 1 and the volume fraction $f = 30\%$.

show the effective material parameters versus size and stiffness ratio for various sets of the interface parameters as

Fig. 8: $\overline{k} = 1,\ \overline{\lambda} = \overline{\mu} = 1$ , Fig. 9: $\overline{k} = 100,\ \overline{\lambda} = \overline{\mu} = 1,$ Fig. 10: $\overline{k} = 100,\ \overline{\lambda} = \overline{\mu} = 100.$.

The left graphs in each box show the effective modulus of interest versus size for three different stiffness ratios of 0.1 (top), 1 (middle) and 10 (bottom). The solid black lines represent the effective response associated with the general interface model and the dashed red and blue lines correspond to the overall response due to the elastic and cohesive interface models, respectively. To compute the effective bulk modulus, an infinitesimal volumetric expansion is prescribed on the microstructure and the distribution of the relevant stress component $\boldsymbol{\sigma}_{xx}$ is shown. On the other hand, in order to compute the effective shear modulus, an infinitesimal simple shear is prescribed on the microstructure and the distribution of the stress component of relevance $\boldsymbol{\sigma}_{xy}$ is given. A generic comparison of the elastic, cohesive and general interfaces at different sizes and stiffness ratios are provided, for the sake of completeness. Note, *the critical size is only obtained if the interface*

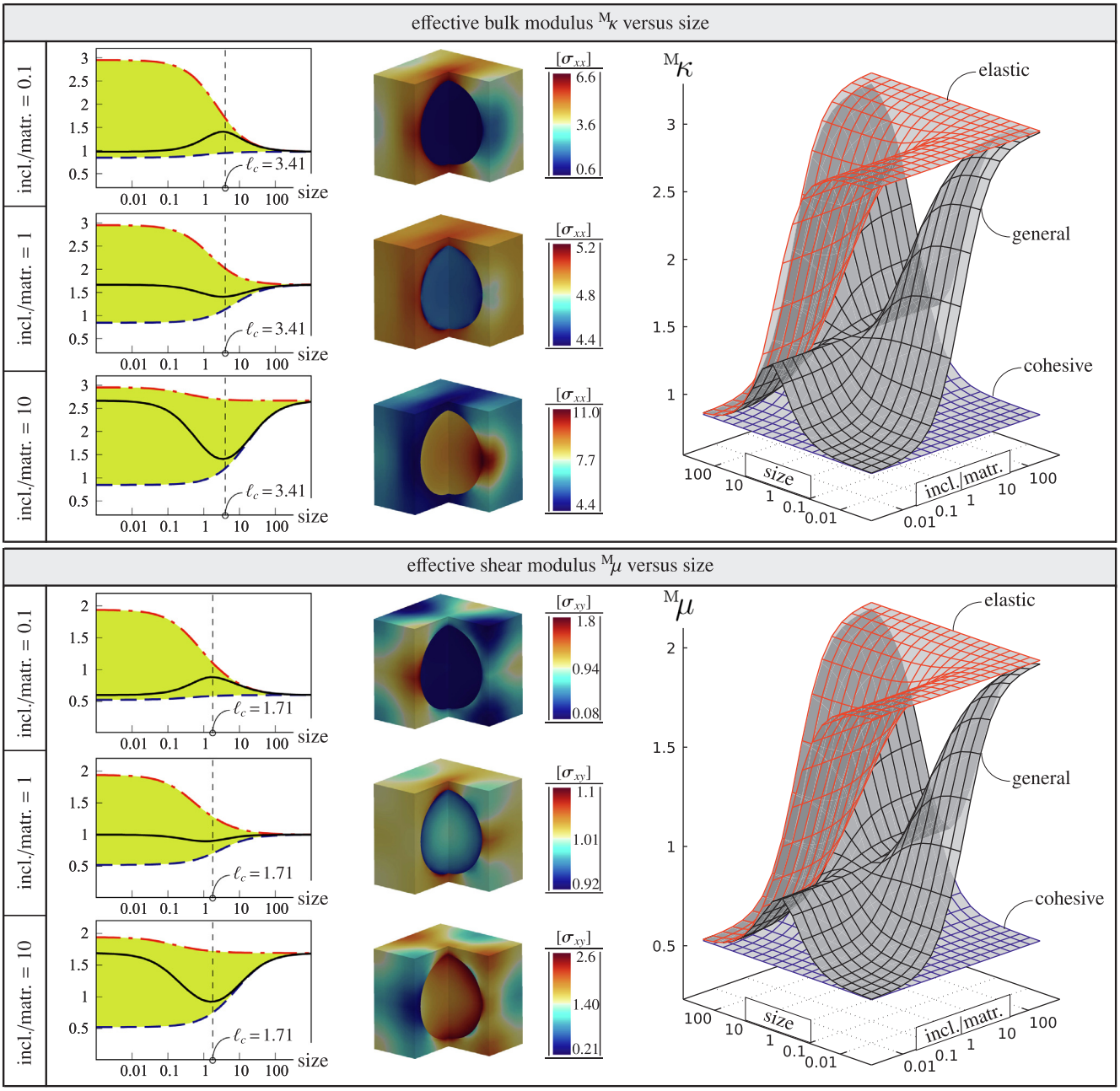


**Fig. 8.** Effective bulk and shear moduli $^{M}\kappa$ and $^{M}\mu$, respectively, versus size and stiffness ratio for elastic, cohesive and general interfaces for interface parameters $\overline{k} = 1$ and $\overline{\lambda} = \overline{\mu} = 1$. The distribution of the stress throughout the RVE is shown for the general interface model at size = 100.

*model is general* and entirely absent for both the cohesive and elastic interface models. Comparing the results for the effective bulk and shear moduli, it can be seen that *the critical size for the effective bulk modulus is not identical to that associated with the effective shear modulus*. Also, according to the observations in Figs. 8–10, we can draw the conclusion that not only *the critical size depends solely on the interface parameters* but also *it is proportional to the square root of the cohesive-to-elastic interface parameters*.

***The overall response due to the general interface model is bounded by those associated with the cohesive and elastic interface models.*** Figs. 8–10 show that for a fixed set of interface parameters, the overall response due to the general interface model is bounded between those associated with the cohesive and elastic interfaces from top and bottom, respectively. Therefore, the elastic and cohesive interface models can be interpreted as the upper and lower bounds of the general interface model, respectively, which shall be compared with the discussion on Fig. 6. Furthermore, *all the effective responses coincide when the size of the micro-structure is very large*. This is expected since the interface effects are proportional to the area-to-volume ratio, hence diminishing at large sizes of the micro-structure.

***General interface model renders a complex combination of both smaller-stiffer and larger-stiffer trends.*** According to the results furnished throughout Figs. 8–10, the elastic interface model shows a smaller-stiffer trend opposite to the cohesive interface model that leads to larger-stiffer behavior regardless of the stiffness ratio. However, this is not the case for the general interface model. The general interface model shows both the smaller-stiffer and larger-stiffer trends resulting in a *critical size* at which its trend reverses. As it can be seen, the overall response due to the general interface model is highly non-linear, relatively complicated and in general unpredictable.

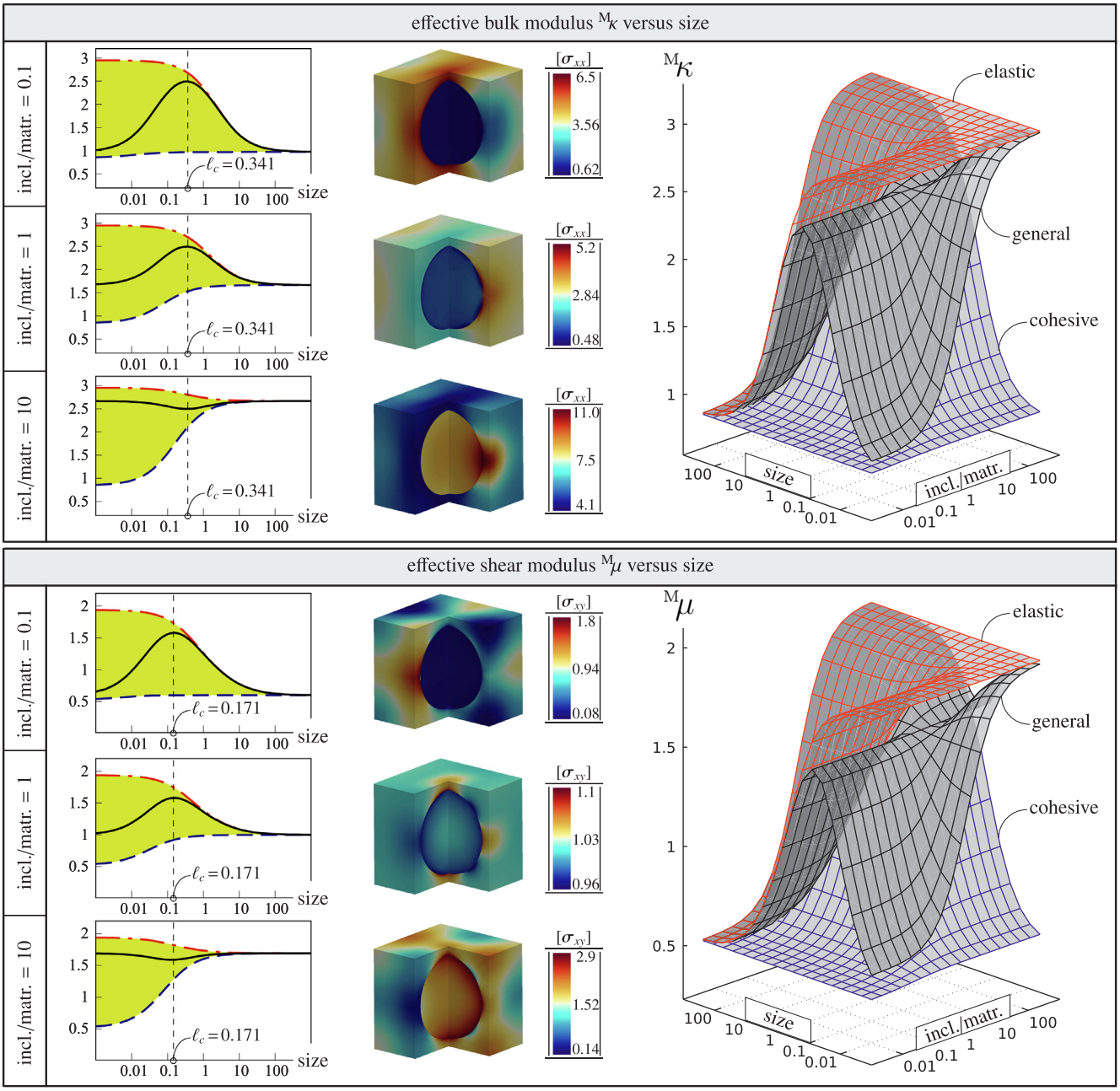


**Fig. 9.** Effective bulk and shear moduli $^{M}\kappa$ and $^{M}\mu$, respectively, versus size and stiffness ratio for elastic, cohesive and general interfaces for interface parameters $\bar{k} = 100$ and $\bar{\lambda} = \bar{\mu} = 1$. The distribution of the stress throughout the RVE is shown for the general interface model at size = 100.

## 4. Conclusion

The overall behavior of particulate composites endowed with generalized interfaces in their micro-structure has been investigated via three-dimensional computational simulations using interface-enhanced finite element method, for a broad range of parameters. Throughout a comprehensive set of numerical examples, the role of various parameters on the effective material response has been examined via computational homogenization. Based on our numerical analysis, we identify a number of uncommon and extraordinary characteristics present due to accounting for interfaces, otherwise missing in the classical computational homogenization. In particular, we report (i) size-dependent effective material response, (ii) identical material response at different volume fractions, (iii) a critical size where the overall response is independent of the stiffness ratio, (iv) the bounds on the overall response and (v) both smaller-stiffer and larger-stiffer trends. The aforementioned observations brings us to the conclusion that the general interface model is a distinctive model to capture size-dependent material behavior and undoubtedly, such complex features show the enormous potential of the general interface model as a versatile tool to design composites with unique mechanical properties. We believe that this manuscript reveals several unfamiliar aspects of the composites embedding interfaces, for the first time, and provides a deeper understanding of the size-dependent behavior of materials which in turn, paves the way towards computational material design accounting for size effects.

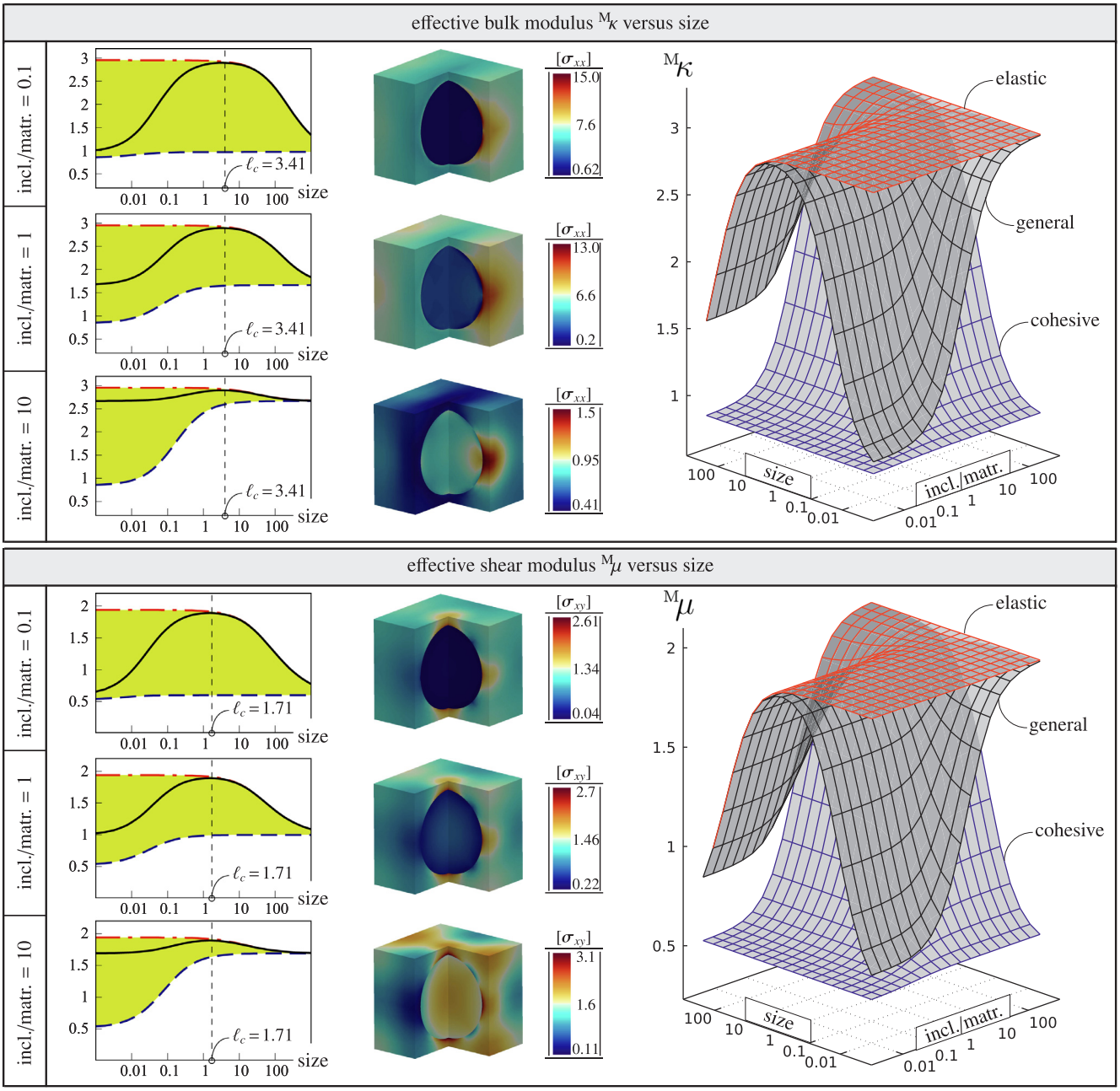


**Fig. 10.** Effective bulk and shear moduli $^{M}\kappa$ and $^{M}\mu$, respectively, versus size and stiffness ratio for elastic, cohesive and general interfaces for interface parameters $\bar{k} = 100$ and $\bar{\lambda} = \bar{\mu} = 100$. The distribution of the stress throughout the RVE is shown for the general interface model at size = 100.

## CRediT authorship contribution statement

**Soheil Firooz:** Writing - original draft, Visualization, Conceptualization, Methodology, Supervision, Writing - review & editing.

## References

[1] R. Hill, On constitutive macro-variables for heterogeneous solids at finite strain, Proc. R. Soc. A: Math. Phys. Eng. Sci. 326 (1972) 131–147.
[2] R.W. Ogden, On the overall moduli of non-linear elastic composite materials, J. Mech. Phys. Solids 22 (1974) 541–553.
[3] R. Hill, Elastic properties of reinforced solids: Some theoretical principles, J. Mech. Phys. Solids 11 (1963) 357–372.
[4] Z.F. Khisaeva, M. Ostoja-Starzewski, On the size of RVE in finite elasticity of random composites, J. Elast. 85 (2006) 153–173.
[5] I. Temizer, T.I. Zohdi, A numerical method for homogenization in non-linear elasticity, Comput. Mech. 40 (2007) 281–298.
[6] I.M. Gitman, H. Askes, E.C. Aifantis, The representative volume size in static and dynamic micro-macro transitions, Int. J. Fract. 135 (2005) 3–9.
[7] T. Kanit, S. Forest, I. Galliet, V. Mounoury, D. Jeulin, Determination of the size of the representative volume element for random composites: statistical and numerical approach, Int. J. Solids Struct. 40 (2003) 3647–3679.
[8] Z. Hashin, S. Shtrikman, A variational approach to the theory of the elastic behaviour of multiphase materials, J. Mech. Phys. Solids 11 (1963) 127–140.
[9] Z. Hashin, B.W. Rosen, The eleastic moduli of fiber-reinforced materials, J. Appl. Mech. 31 (1964) 223–232.
[10] R. Hill, Theory of mechanical properties of fibre-strengthened materials: I. Elastic behaviour, J. Mech. Phys. Solids 12 (1964) 199–212.
[11] R. Hill, A self-consistent mechanics of composite materials, J. Mech. Phys. Solids 13 (1965) 213–222.
[12] L.J. Walpole, On the overall elastic moduli of composite materials, J. Mech. Phys. Solids 17 (1969) 235–251.
[13] T. Mori, K. Tanaka, Average stress in matrix and average elastic energy of materials with misfitting inclusions, Acta Metall. 21 (1973) 571–574.
[14] J.R. Willis, Bounds and self-consistent estimates for the overall properties of anisotropic composites, J. Mech. Phys. Solids 25 (1977) 185–202.
[15] S. Nemat-Nasser, T. Iwakuma, Elastic-plastic composites at finite strains, Int. J.

Solids Struct. 21 (1985) 55–65.
[16] J.R. Willis, On methods for bounding the overall properties of ninlinear composites, J. Mech. Phys. Solids 39 (1991) 73–86.
[17] P. Ponte Castañeda, The effective mechanical properties of nonlinear isotropic composites, J. Mech. Phys. Solids 39 (1991) 45–71.
[18] S. Torquato, Random heterogeneous media: microstructure and improved bounds on effective properties, Appl. Mech. Rev. 44 (1991) 37–76.
[19] G. Wang, M.J. Pindera, Locally-exact homogenization theory for transversely isotropic unidirectional composites, Mech. Res. Commun. 78 (2016) 2–14.
[20] A. Ramírez-Torres, S. Di Stefano, A. Grillo, R. Rodríguez-Ramos, J. Merodio, R. Penta, An asymptotic homogenization approach to the microstructural evolution of heterogeneous media, Int. J. Non-Linear Mech. 106 (2018) 245–257.
[21] M.G.D. Geers, V.G. Kouznetsova, T.J. Massart, I. Özdemir, E. Coenen, W.A.M. Brekelmans, R. Peerlings, Computational homogenization of structures and materials, HAL, 2009.
[22] I. Özdemir, W.A.M. Brekelmans, M.G.D. Geers, Computational homogenization for heat conduction in heterogeneous solids, Int. J. Numer. Meth. Eng. 73 (2008) 185–204.
[23] J. Yvonnet, E. Monteiro, Q.C. He, Computational homogenization method and reduced database model for hyperelastic heterogeneous structures, Int. J. Multiscale Comput. Eng. 11 (2013) 201–225.
[24] A. Javili, G. Chatzigeorgiou, A.T. McBride, P. Steinmann, C. Linder, Computational homogenization of nano-materials accounting for size effects via surface elasticity, GAMM Mitteilungen 38 (2015) 285–312.
[25] B.A. Le, J. Yvonnet, Q.C. He, Computational homogenization of nonlinear elastic materials using neural networks, Int. J. Numer. Meth. Eng. 104 (2015) 1061–1084.
[26] S. Saeb, P. Steinmann, A. Javili, Aspects of computational homogenization at finite deformations: a unifying review from Reuss' to Voigt's bound, Appl. Mech. Rev. 68 (2016) 050801 .
[27] P. Kanouté, D.P. Boso, J.L. Chaboche, B.A. Schrefler, Multiscale methods for composites: a review, Arch. Comput. Methods Eng. 16 (2009) 31–75.
[28] N. Charalambakis, G. Chatzigeorgiou, Y. Chemisky, F. Meraghni, Mathematical homogenization of inelastic dissipative materials: a survey and recent progress, Continuum Mech. Thermodyn. 30 (2018) 1–51.
[29] M.J. Pindera, H. Khatam, A.S. Drago, Y. Bansal, Micromechanics of spatially uniform heterogeneous media: a critical review and emerging approaches, Compos. Part B: Eng. 40 (2009) 349–378.
[30] S. Firooz, S. Saeb, G. Chatzigeorgiou, F. Meraghni, P. Steinmann, A. Javili, Systematic study of homogenization and the utility of circular simplified representative volume element, Math. Mech. Solids.https://doi.org/10.1177/1081286518823834.
[31] N. Daher, G.A. Maugin, The method of virtual power in continuum mechanics application to media presenting singular surfaces and interfaces, Acta Mech. 60 (1986) 217–240.
[32] E. Sanchez-Palencia, Comportement limite d'un probleme de transmissiona travers une plaque faiblement conductrice, Compt. Rendus Math. Acad. Sci. 270 (1970) 1026–1028.
[33] H.P. Huy, E. Sanchez-Palencia, Phénomènes de transmission à travers des couches minces de conductivitéélevée, J. Math. Anal. Appl. 47 (1974) 284–309.
[34] P. Sharma, S. Ganti, N. Bhate, Effect of surfaces on the size-dependent elastic state of nano-inhomogeneities, Appl. Phys. Lett. 82 (2003) 535–537.
[35] H.L. Duan, J. Wang, B.L. Karihaloo, Theory of Elasticity at the Nanoscale vol. 42, Elsevier, 2009.
[36] D. Davydov, A. Javili, P. Steinmann, On molecular statics and surface-enhanced continuum modeling of nano-structures, Comput. Mater. Sci. 69 (2013) 510–519.
[37] S. Saeb, P. Steinmann, A. Javili, Bounds on size-dependent behaviour of composites, Philos. Mag. 98 (2018) 437–463.
[38] S. Saeb, P. Steinmann, A. Javili, Applications of general interfaces to design nanocomposites, Int. J. Solids Struct.
[39] Q. Chen, G. Wang, M.J. Pindera, Homogenization and localization of nanoporous composites – a critical review and new developments, Compos. Part B: Eng. 155 (2018) 329–368.
[40] M.E. Gurtin, A.I. Murdoch, A continuum theory of elastic material surfaces, Arch. Ration. Mech. Anal. 57 (1975) 291–323.
[41] M.E. Gurtin, A.I. Murdoch, Surface stress in solids, Int. J. Solids Struct. 14 (1978) 431–440.
[42] A.I. Murdoch, A thermodynamical theory of elastic material interfaces, Q. J. Mech. Appl. Mech. 29 (1976) 245–275.
[43] D.J. Steigmann, R.W. Ogden, Plane deformations of elastic solids with intrinsic boundary elasticity, Proc. R. Soc. A: Math. Phys. Eng. Sci. 453 (1997) 853–877.
[44] Z. Han, S.G. Mogilevskaya, D. Schillinger, Local fields and overall transverse properties of unidirectional composite materials with multiple nanofibers and Steigmann-Ogden interfaces, Int. J. Solids Struct. 147 (2018) 166–182.
[45] Y. Benveniste, T. Miloh, Imperfect soft and stiff interfaces in two-dimensional elasticity, Mech. Mater. 33 (2001) 309–323.
[46] P. Sharma, S. Ganti, Size-dependent Eshelby's tensor for embedded nano-inclusions incorporating surface/interface energies, J. Appl. Mech. 71 (2004) 663–671.
[47] H.L. Duan, J. Wang, Z.P. Huang, B.L. Karihaloo, Eshelby formalism for nano-inhomogeneities, Proc. R. Soc. A: Math. Phys. Eng. Sci. 461 (2005) 3335–3353.
[48] H.L. Duan, J. Wang, Z.P. Huang, B.L. Karihaloo, Size-dependent effective elastic constants of solids containing nano-inhomogeneities with interface stress, J. Mech. Phys. Solids 53 (2005) 1574–1596.
[49] L.H. He, Self-strain of solids with spherical nanovoids, Appl. Phys. Lett. 88 (2006) 12–15.
[50] Z.P. Huang, L. Sun, Size-dependent effective properties of a heterogeneous material with interface energy effect: from finite deformation theory to infinitesimal strain analysis, Acta Mech. 190 (2007) 151–163.
[51] J. Yvonnet, H. Le Quang, Q.C. He, An XFEM/level set approach to modelling surface/interface effects and to computing the size-dependent effective properties of nanocomposites, Comput. Mech. 42 (2008) 119–131.
[52] H. Le Quang, Q.C. He, Variational principles and bounds for elastic inhomogeneous materials with coherent imperfect interfaces, Mech. Mater. 40 (2008) 865–884.
[53] S. Brisard, L. Dormieux, D. Kondo, Hashin-Shtrikman bounds on the shear modulus of a nanocomposite with spherical inclusions and interface effects, Comput. Mater. Sci. 50 (2010) 403–410.
[54] V.I. Kushch, S.G. Mogilevskaya, H.K. Stolarski, S.L. Crouch, Elastic interaction of spherical nanoinhomogeneities with GurtinMurdoch type interfaces, J. Mech. Phys. Solids 59 (2011) 1702–1716.
[55] G. Chatzigeorgiou, A. Javili, P. Steinmann, Multiscale modelling for composites with energetic interfaces at the micro- or nanoscale, Math. Mech. Solids 20 (2015) 1130–1145.
[56] M. Dai, P. Schiavone, C.F. Gao, Prediction of the stress field and effective shear modulus of composites containing periodic inclusions incorporating interface effects in anti-plane shear, J. Elast. 125 (2016) 217–230.
[57] X. Gao, Z. Huang, D. Fang, Curvature-dependent interfacial energy and its effects on the elastic properties of nanomaterials, Int. J. Solids Struct. 113–114 (2017) 100–107.
[58] D.S. Dudgale, Yielding of steel sheets containing slits, J. Mech. Phys. Solids 8 (1960) 100–104.
[59] G.I. Barenblatt, The mathematical theory of equilibrium cracks in brittle materials, Adv. Appl. Mech. 7 (1962) 55–129.
[60] A. Needleman, A continuum model for void nucleation by inclusion debonding, J. Appl. Mech. 54 (1987) 525–531.
[61] A. Javili, A note on traction continuity across an interface in a geometrically nonlinear framework, Math. Mech. Solids.https://doi.org/10.1177/1081286518766980.
[62] Y. Benveniste, The effective mechanical behaviour of composite materials with imperfect contact between the constituents, Mech. Mater. 4 (1985) 197–208.
[63] J.D. Achenbach, H. Zhu, Effect of interfacial zone on mechanical behavior and failure of fiber-reinforced composites, J. Mech. Phys. Solids 37 (1989) 381–393.
[64] Z. Hashin, Thermoelastic properties of particulate composites with imperfect interface, J. Mech. Phys. Solids 39 (1991) 745–762.
[65] Z. Hashin, Thermoelastic properties of fiber composites with imperfect interface, Mech. Mater. 8 (1990) 333–348.
[66] R. Lipton, B. Vernescu, Variational methods, size effects and extremal microgeometries for elastic composites with imperfect interface, Math. Models Methods Appl. Sci. 5 (1995) 1139–1173.
[67] H.L. Duan, J. Wang, Z.P. Huang, Z.Y. Luo, Stress concentration tensors of inhomogeneities with interface effects, Mech. Mater. 37 (2005) 723–736.
[68] H. Tan, Y. Huang, C. Liu, P.H. Geubelle, The Mori-Tanaka method for composite materials with nonlinear interface debonding, Int. J. Plast 21 (2005) 1890–1918.
[69] F. Fritzen, M. Leuschner, Nonlinear reduced order homogenization of materials including cohesive interfaces, Comput. Mech. 56 (2015) 131–151.
[70] Z. Hashin, Thin interphase/imperfect interface in elasticity with application to coated fiber composites, J. Mech. Phys. Solids 50 (2002) 2509–2537.
[71] Y. Benveniste, Models of thin interphases and the effective medium approximation in composite media with curvilinearly anisotropic coated inclusions, Int. J. Eng. Sci. 72 (2013) 140–154.
[72] Y. Benveniste, A general interface model for a three-dimensional curved thin anisotropic interphase between two anisotropic media, J. Mech. Phys. Solids 54 (2006) 708–734.
[73] P. Bövik, On the modelling of thin interface layers in elastic and acoustic scattering problems, Q. J. Mech. Appl. Math. 47 (1994) 17–42.
[74] J. Wang, H.L. Duan, Z. Zhang, Z.P. Huang, An anti-interpenetration model and connections between interphase and interface models in particle-reinforced composites, Int. J. Mech. Sci. 47 (2005) 701–718.
[75] Y. Koutsawa, A. Karatrantos, W. Yu, D. Ruch, A micromechanics approach for the effective thermal conductivity of composite materials with general linear imperfect interfaces, Compos. Struct. 200 (2018) 747–756.
[76] S.T. Gu, Q.C. He, Interfacial discontinuity relations for coupled multifield phenomena and their application to the modeling of thin interphases as imperfect interfaces, J. Mech. Phys. Solids 59 (2011) 1413–1426.
[77] S.T. Gu, J.T. Liu, Q.C. He, Size-dependent effective elastic moduli of particulate composites with interfacial displacement and traction discontinuities, Int. J. Solids Struct. 51 (2014) 2283–2296.
[78] G. Chatzigeorgiou, F. Meraghni, A. Javili, Generalized interfacial energy and size effects in composites, J. Mech. Phys. Solids 106 (2017) 257–282.
[79] F. dell'Isola, A. Romano, On the derivation of thermomechanical balance equations for continuous systems with a nonmaterial interface, Int. J. Eng. Sci. 25 (1987) 1459–1468.
[80] E. Fried, M.E. Gurtin, Thermomechanics of the interface between a body and its environment, Continuum Mech. Thermodyn. 19 (2007) 253–271.
[81] A. Javili, A. McBride, P. Steinmann, Thermomechanics of solids with lower-dimensional energetics: on the importance of surface, interface, and curve structures at the nanoscale. A unifying review, Appl. Mech. Rev. 65 (2013) 010802 .
[82] A. Javili, P. Steinmann, J. Mosler, Micro-to-macro transition accounting for general imperfect interfaces, Comput. Methods Appl. Mech. Eng. 317 (2017) 274–317.